Inorganic Chemistry
Article

Inorg. Chem. **2009**, *48*, 11017–11023 **11017**
DOI: 10.1021/ic901167u

Kinetic Control of Intralayer Cobalt Coordination in Layered Hydroxides: $Co^{oct}_{1-0.5x}Co^{tet}_{x}(OH)_2(Cl)_x(H_2O)_n$

James R. Neilson,[†,‡,§] Birgit Schwenzer,[‡,§] Ram Seshadri,[‡,∥] and Daniel E. Morse[*,†,‡,§]

[†] *Biomolecular Science & Engineering, University of California Santa Barbara, California 93106-9611,*
[‡] *Materials Research Laboratory, University of California Santa Barbara, California 93106-5121,*
[§] *Institute for Collaborative Biotechnologies, University of California Santa Barbara, California 93106-5100, and*
[∥] *Materials Department, University of California Santa Barbara, California 93106-5050*

Received June 17, 2009

We report the synthesis and characterization of new structural variants of the isotypic compound with the generic chemical formula, $Co^{oct}_{1-0.5x}Co^{tet}_{x}(OH)_2(Cl)_x(H_2O)_n$, all modifications of an α-$Co(OH)_2$ lattice. We show that the occupancy of tetrahedrally coordinated cobalt sites and associated chloride ligands, *x*, is modulated by the rate of formation of the respective layered hydroxide salts from kinetically controlled aqueous hydrolysis at an air−water interface. This new level of structural control is uniquely enabled by the slow diffusion of a hydrolytic catalyst, a simple technique. Independent structural characterizations of the compounds separately describe various attributes of the materials on different length scales, revealing details hidden by the disordered average structures. The precise control over the population of distinct octahedrally and tetrahedrally coordinated cobalt ions in the lattice provides a gentle, generic method for modulating the coordination geometry of cobalt in the material without disturbing the lattice or using additional reagents. A mechanism is proposed to reconcile the observation of the kinetic control of the structure with competing interactions during the initial stages of hydrolysis and condensation.

Introduction

While layered double hydroxides (LDH) have been well studied,[1] it remains difficult to synthesize and characterize these compounds with extended long-range order and reproducibility because of a high propensity to form defects, both within each layer and between layers, especially in a related species of layered hydroxide salt structures, α-$Co(OH)_2$ (Figure 1a).[1−3] On the basis of a simple CdI_2 lattice,[4] β-$Co(OH)_2$ is a lamellar stack of two-dimensional sheets of edge sharing metal-hydroxyl octahedra, shown on the right in Figure 1b. The α-$Co(OH)_2$ structure Figure 1a, is reported to be a modification of the β-$Co(OH)_2$ lattice that contains vacant metal octahedra, with each vacancy capped by two tetrahedrally coordinated divalent metal ions on each side of the layer.[3,5] These structures are related to the mineral Simonkolleite, $Zn_5(OH)_8(Cl)_2(H_2O)$, with regular ordering of a fixed fraction of tetrahedral sites in the lattice.[6] In these modifications of the layered hydroxide, a neutralizing counteranion and often water are found in the interlayer gallery where they complex the tetrahedral cations or reside in the interstitial space.[2] The positions of these interlayer species are often disordered.[1]

These types of layered cobalt structures often yield fascinating properties relating to the unpaired spins, the crystal field of the cobalt, and the spatial distribution of ions. The color of these compounds may range from a faint pink from octahedrally coordinated cobalt to a dark green-blue from the strongly absorbing tetrahedral cobalt sites in the lattice.[7,8] In a related α-$Co(OH)_2$ compound, $Co_5(OH)_8(NO_3)_2(H_2O)_2$, *p*-type photoconductivity has been observed[9] and has recently been utilized to fabricate photovoltaic devices using a hybrid inorganic−organic architecture.[10] It therefore is important to accurately describe the structure and

*To whom correspondence should be addressed. E-mail: d_morse@lifesci.ucsb.edu. Fax: +001-805-893-7998. Phone:+001-805-893-7442.

(1) Rives, V. *Layered Double Hydroxides: Present and Future*; Nova: Hauppauge, NY, 2001.
(2) Evans, D. G.; Slade, R. C. T. Structural Aspects of Layered Double Hydroxides. In *Layered Double Hydroxides; Structure and Bonding*; Springer: Berlin, 2006; pp 1−87.
(3) Arizaga, G. G. C.; Satyanarayana, K. G.; Wypych, F. *Solid State Ionics* **2007**, *178*, 1143–1162.
(4) Megaw, H. D. *Crystal structures: a working approach*; Saunders: Philadelphia, 1973.
(5) Ma, R.; Liu, Z.; Takada, K.; Fukuda, K.; Ebina, Y.; Bando, Y.; Sasaki, T. *Inorg. Chem.* **2006**, *45*, 3964–3969.
(6) Hawthorne, F.; Sokolova, E. *Can. Mineral.* **2002**, *40*, 939–946.
(7) Lever, A. B. P. *Inorganic electronic spectroscopy*; Elsevier: New York, 1968.
(8) Liu, Z.; Ma, R.; Osada, M.; Takada, K.; Sasaki, T. *J. Am. Chem. Soc.* **2005**, *127*, 13869–13874.
(9) Schwenzer, B.; Roth, K. M.; Gomm, J. R.; Murr, M.; Morse, D. E. *J. Mater. Chem.* **2006**, *16*, 401–407.
(10) Schwenzer, B.; Neilson, J. R.; Sivula, K.; Woo, C.; Fréchet, J. M. J.; Morse, D. E. *Thin Solid Films* **2009**, *517*, 5722–5727.

Published on Web 10/26/2009

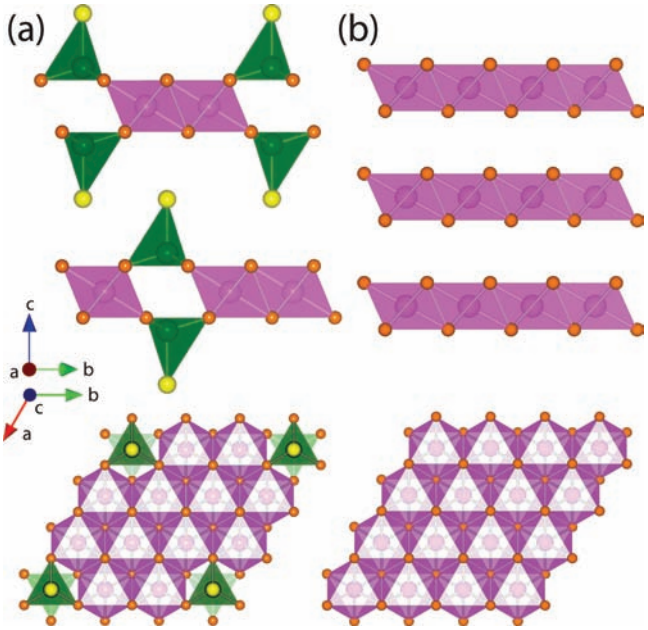

Figure 1. Schematic representations of (a) α-$Co(OH)_2$ and (b) β-$Co(OH)_2$ structures illustrating the variable incorporation of tetrahedral sites in the lattice and increased interlayer spacing in the α-$Co(OH)_2$ structure. (Pink: octahedral cobalt; green: tetrahedral cobalt; orange: oxygen; yellow: chlorine; hydrogen and water omitted for clarity).

population of the absorption centers to better understand these and related electromagnetic and optoelectronic phenomena.

The structures of layered cobalt hydroxides are often described from powder X-ray diffraction patterns consisting of broad peaks corresponding to the interlamellar spacing and their harmonics.[1−3] The broadening and asymmetry of the reflections arise from small particle sizes, interstratification, and stacking faults[11−13] that are qualitatively described using programs such as DiFFaX.[14] However, the analyses do not allow a description of atomic details of the intralayer geometry.

Improvements in synthetic techniques based on the slow hydrolysis of soluble precursors[5,8,9,15] have allowed long-range ordering of the lattice in α-$Co(OH)_2$ compounds, producing structures suitable for structural refinement in some cases.[5] Additionally, utilization of diffusion across the air−water interface provides a method to isolate material produced under kinetic control without organic reagents.[9,15] The use of interfaces to spatially and temporally control the growth of nanostructured thin films with diffusion of soluble reactants through the adjoining media is a powerful technique for the synthesis of many different materials.[16] In this study, we demonstrate a new ability of this technique to control the structure of the resulting material at the atomic level.

By using slow diffusion across an air−water interface, we specifically achieve kinetic control of a variable intralayer cobalt coordination in the layered hydroxide salt, $Co^{oct}_{1-0.5x}Co^{tet}_{x}(OH)_2(Cl)_x(H_2O)_n$. Structural characterization on multiple length scales in conjunction with compositional analysis shows a systematic trend: faster reactions decrease the population of tetrahedral sites in the lattice, x. However, slow reactions approaching equilibrium conditions have a similar effect. These newly observed variations in the structure are a direct product of the slow, controlled hydrolysis and condensation. A mechanism is proposed to reconcile the kinetic competition between hydrolysis of soluble octahedral cobalt complexes and condensation of these complexes with transiently formed tetrahedral cobalt complexes stabilized by the chloride ligand. These structural observations and method for modulating the structure have relevance and implications for the magnetic, optical, and electronic behavior of α-$Co(OH)_2$ structures, independent of intercalated counteranion.

Experimental Section

Synthesis. All starting materials used in this study are commercially available (Sigma Aldrich Co. or Alfa Aesar, unless noted otherwise) and were used without further purification. All water used was filtered and deionized to a resistivity greater than 18 MΩ cm^{-1} using a Milli-Q purification system. Free-standing thin films of $Co_{1+0.5x}(OH)_2(Cl)_x(H_2O)_n$ were prepared by a kinetically controlled, vapor-diffusion catalysis method at room temperature as previously described.[9] Reactions were carried out under ambient conditions, in a sealed container (3 L volume) to isolate the reaction chamber from the atmosphere. A 40 mL volume of an aqueous solution of 0.1 M $CoCl_2$ was placed in two Petri dishes, next to a separate Petri dish containing a dilute ammonia solution (8 mL). The ratio of surface areas to volumes of the precursor solution and ammonia solution were each fixed at 56 cm^2 to 40 mL and 28 cm^2 to 8 mL, respectively. Dissolved ammonia concentrations (0.6%, 1.2%, 6%, and 12% v/v $NH_{3(aq)}$) were chosen within a range that yields a thin film at the interface. The ammonia solutions were prepared from dilutions of an ammonium hydroxide solution (30% NH_3 assay; EMD Chemicals, Inc.). Concentrations of ammonia used outside of this range yield either bulk precipitation or no product formation. The reactions were terminated after a continuous thin film was observed at the meniscus of the precursor solution, but before any bulk precipitation was detectable, to retain kinetic control of the reaction and to prevent stoichiometric depletion of any reagents. Compound **1** ($Co_{1.20}(OH)_2(Cl)_{0.40}(H_2O)_{1.1}$) was isolated using the Langmuir−Blodgett technique from a reaction using 0.6% $NH_{3(aq)}$ after 24 h; **2** ($Co_{1.25}(OH)_2(Cl)_{0.5}(H_2O)_{0.4}$) from 1.2% $NH_{3(aq)}$ after 6 h; **3** ($Co_{1.15}(OH)_2(Cl)_{0.31}(H_2O)_{0.3}$) from 6% $NH_{3(aq)}$ after 30 minutes; and **4** ($Co_{1.13}(OH)_2(Cl)_{0.26}(H_2O)_{1.5}$) from 12% $NH_{3(aq)}$ after 5 min. The control amorphous product, **5**, was produced by titration of 8 mL of a 1.2% $NH_{3(aq)}$ solution to 40 mL of a 0.1 M $CoCl_{2(aq)}$ solution while stirring. The isolated product was dried at room temperature for 24 h and was typically ground into a fine powder for further analysis.

Compositional and Structural Characterization. Samples were dissolved in 4% $HNO_{3(aq)}$ solutions for inductively coupled plasma atomic emission spectroscopy (ICP-AES) to determine the amount of cobalt per formula unit using a Thermo iCAP 6300 instrument calibrated with 50 and 100 ppm Co standards from dissolved $CoCl_2 \cdot 6H_2O$ (4% $HNO_{3(aq)}$) and a 10 ppm quality control mixed metal standard (High Purity Standards). Since ICP-AES is not suitable for measuring chlorine content, the chloride to cobalt ratio of compounds **1**−**4** was determined with two methods: energy dispersive spectroscopy (EDS) and

(11) Rajamathi, M.; Kamath, P. V.; Seshadri, R. *Mater. Res. Bull.* **2000**, *35*, 271–278.
(12) Ramesh, T. N.; Rajamathi, M.; Kamath, P. V. *Solid State Sci.* **2003**, *5*, 751–756.
(13) Ramesh, T. N.; Rajamathi, M.; Kamath, P. V. *J. Solid State Chem.* **2006**, *179*, 2386–2393.
(14) Treacy, M.; Deem, M.; Newsam, J. *Proc. R. Soc. London, Ser. A* **1991**, *433*, 499.
(15) Du, Y.; O'Hare, D. *J. Phys. Chem. Solids* **2008**, *69*, 1040–1043.
(16) Gautam, U. K.; Ghosh, M.; Rao, C. N. R. *Chem. Phys. Lett.* **2003**, *381*, 1–6.

Table 1. Chemical Analysis Results from XPS, EDS, and Inductively Coupled Plasma Atomic Emission Spectroscopy (ICP) Used to Determine the Chemical Formulae of Each Compound

prod.	ammonia conc. (v/v)	cobalt per formula mass (ICP, ppm)	Cl/Co ratio (EDS, mol %)	Cl/Co ratio (XPS, mol %)	calculated formulas (from ICP, EDS) $Co_{1-0.5x}^{oct}Co_{x}^{tet}(OH)_2(Cl)_x(H_2O)_n$
1	0.6% $NH_{3(aq)}$	42.0	33	25	$Co_{0.80}^{oct}Co_{0.40}^{tet}(OH)_2(Cl)_{0.40}(H_2O)_{1.1}$
2	1.2% $NH_{3(aq)}$	53.0	40	33	$Co_{0.75}^{oct}Co_{0.50}^{tet}(OH)_2(Cl)_{0.50}(H_2O)_{0.4}$
3	6% $NH_{3(aq)}$	57.4	27	23	$Co_{0.84}^{oct}Co_{0.31}^{tet}(OH)_2(Cl)_{0.31}(H_2O)_{0.3}$
4	12% $NH_{3(aq)}$	49.4	23	15	$Co_{0.87}^{oct}Co_{0.26}^{tet}(OH)_2(Cl)_{0.26}(H_2O)_{1.5}$

X-ray photoelectron spectroscopy (XPS). The elemental microanalysis with EDS was acquired on a Tescan Vega 5130 SEM using an iXRF energy dispersive spectrometer operating at 20 kV with a 4.0 s time constant, counting for 100 s live time. The average of 5 locations on non-coated samples at a 5000× operating magnification at a constant working distance was used to compute the reported values (Table 1). The surface composition was studied using XPS by comparing the peak areas (Cl 2p and Co 2p) from survey spectra. Each spectrum was acquired on a Kratos Axis Ultra with a monochromated aluminum anode and was calibrated using the appropriate instrumental scaling factors for each core level. XPS data was analyzed using CasaXPS. Decomposition of the core-level of the Co 2p peaks into different components was avoided to avoid interpretation of shakeup satellites and background subtraction and is presented in the Supporting Information. The respective chemical formulas, summarized in Table 1, were solved according to the generic formula $Co_{1+0.5x}(OH)_2(Cl)_x(H_2O)_n$ to retain charge neutrality and the α-$Co(OH)_2$ structure.

Structural Analysis and Instrumentation. Scanning electron microscopy (SEM) of gold sputtered samples was performed on a Tescan Vega 5130 SEM. Low intensity powder X-ray diffraction was performed using a Philips XPERT thin-film diffractometer with monochromatic Cu Kα radiation (λ = 1.540 Å) and a graphite monochromator inline with the detector to minimize cobalt X-ray fluorescence, utilizing the Bragg-Bentano geometry.

High resolution synchrotron powder diffraction data were collected for **1** and **4** using beamline 11-BM at the Advanced Photon Source (APS), Argonne National Laboratory, using an average wavelength of 0.4128(2) Å.[17] Discrete detectors covering an angular range from −6 to 16° 2θ are scanned over a 34° 2θ range, with data points collected every 0.001° 2θ and scan speed of 0.01° s^{-1}. Data are collected while continually scanning the diffractometer 2θ arm. A mixture of NIST standard reference materials, Si (SRM 640c) and Al_2O_3 (SRM 676) is used to calibrate the instrument, where the Si lattice constant determines the wavelength for each detector. Corrections are applied for detector sensitivity, 2θ offset, small differences in wavelength between detectors, and the source intensity, as noted by the ion chamber before merging the data into a single set of intensities evenly spaced in 2θ. Structures were refined with the Rietveld method employed by the General Structure Analysis System (GSAS),[18,19] initialized using the structural model from Ma et al.,[5] and were visualized using the software VESTA.[20] The refinement was completed by adjusting the profile shape with the major 003 and 006 reflections, then refining the unit cell, positions, and thermal parameters beginning with the heaviest elements. The site occupancies were then constrained with $g_{Co}{}^{oct} = 1 - g_{Co}{}^{tet}$, while manually equating the chloride occupancy to that of the tetrahedrally coordinated cobalt site. When completed, all available structural parameters were allowed to refine simultaneously.

Raman spectra of powder samples were recorded using a LabRAM Aramis Raman microscope spectrometer using a 785 nm excitation laser damped with a neutral density filter to eliminate sample decomposition or oxidation. Diffuse reflectance spectra were recorded from powder samples supported in an inert $BaSO_4$ matrix (95 wt %) to normalize scattering contributions in a Shimadzu UV 3600 UV−vis−NIR spectrometer with an integrating sphere.

Results and Discussion

When using the vapor-phase diffusion of a volatile catalyst to promote hydrolysis and condensation in a metal salt solution,[9] there is great variability in the structure and morphology of the product as a function of the rate of the reaction. The reaction predominantly occurs at or near the interface of the precursor solution and proceeds with kinetic control. It does not reach completion since the reactions are halted before bulk precipitation occurs. Therefore, systematic variation of the reaction rate is accomplished by changing the concentration of ammonia presented in the vapor-source. Slower reactions result from decreased ammonia concentrations. This procedure permitted the synthesis of isotypic α-$Co(OH)_2$ compounds **1**−**4** with varied intralayer structures.

Chemical Composition. Stoichiometric analysis of the products from each reaction condition (**2**−**4**) reveals a general trend in which slow reactions incorporate more chloride ions into the lattice, with the exception of the product of the slowest reaction, **1**. EDS and XPS allow quantification of the ratio of chlorine to cobalt as a function of ammonia concentration during synthesis (Table 1). The Cl/Co ratios measured by EDS are used to compute the chemical formulas of each compound, since XPS is surface sensitive. While the XPS measurements observe less relative chloride content than the EDS microanalysis, both techniques show the same trend as a function of ammonia concentration (Table 1). The systematic correlation of the chloride concentration with some slight modifications of the atomic lattice does not lead to drastic deviation in the average structure as determined by X-ray diffraction (Figure 2). A previous analysis of the α-$Co(OH)_2$ structure concluded that each tetrahedrally coordinated cobalt in the lattice is capped at a vertex by one chloride ligand residing in the interlayer gallery.[5] Thus, we conclude that a concomitant increase in the population of tetrahedral sites in the lattice occurs with increased chloride content. To remain consistent with previous findings[5] and retain charge neutrality, the generic chemical formula must be $Co_{1+0.5x}(OH)_2(Cl)_x(H_2O)_n$, with the chloride content constrained from $0 < x \leq 0.5$ with variable water content. For this study, the variable x is determined from the chloride to cobalt ratio measured by EDS, with the amount of cobalt per formula unit quantified by inductively coupled plasma atomic emission spectroscopy (ICP-AES), thereby defining n,

(17) Wang, J.; Toby, B. H.; Lee, P. L.; Ribaud, L.; Antao, S. M.; Kurtz, C.; Ramanathan, M.; Dreele, R. B. V.; Beno, M. A. *Rev. Sci. Instrum.* **2008**, *79*, 085105.
(18) Larson, A. C.; Dreele, R. B. V. *Los Alamos National Laboratory Report LAUR* **2000**, 86–748.
(19) Toby, B. H. J. *Appl. Crystallogr.* **2001**, *34*, 210–213.
(20) Momma, K.; Izumi, F. J. *Appl. Crystallogr.* **2008**, *41*, 653–658.

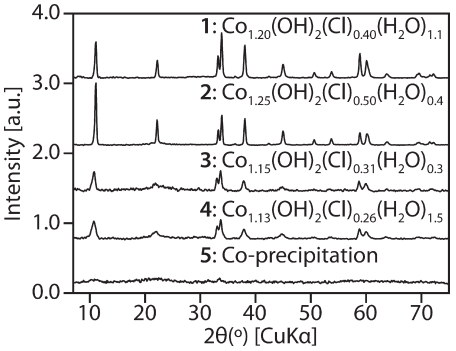

Figure 2. Powder X-ray diffraction profiles of compounds **1**−**5** (in order of increasing hydrolysis rate), highlighting the increased disorder and retention of average structure as a function of hydrolysis rate for compounds **1**−**4**.

the water content. Schematic structures in Figure 1 illustrate the correlation between chloride content and tetrahedral sites in the lattice, thereby decreasing the connectivity of octahedral sites in each layer.

High-resolution XPS was explored to measure the cobalt 2p and chlorine 2p core electron binding energies. The Cl 2p XPS spectra indicated one species of chlorine present (Supporting Information, Figure S1). Decomposition of the Co 2p XPS spectra into different components (Supporting Information, Figure S2) indicates the presence of at least two distinct species of cobalt, but quantification and precise position location of each species is unreliable because of the difficulty in the assignment of shakeup satellite peaks overlapping in the 2p sub-bands in addition to the subtraction of the background over the wide peak region.[21] While this decomposition of the XPS data for two species does not confirm an absence of Co^{3+}, its potential presence is limited to sub-stoichiometric quantities.[9] Using conservative background functions (Supporting Information, Figure S2), a trend in the relative ratios of each cobalt species (I: Co^{oct}; II: Co^{tet}) is observed in support of the fractional occupancy of 4-fold coordinated cobalt that varies with reaction rate (Supporting Information, Table S1). However, the absolute values are insignificant as the percentage of presumed tetrahedrally coordinated cobalt exceeds that of the theoretically possible value (40%). This result may also arise from a surface enrichment of the 4-coordinated cobalt species; however, this necessitates further study.

Long-Range Order. Powder X-ray diffraction (XRD) provides an excellent probe of the atomic structure and long-range order. Looking from top to bottom in Figure 2, the overall diffraction profiles do not change; however, faster reaction rates yield products (**1** to **4**) with increased disorder. In layered hydroxides, broadened and asymmetric reflections are attributed to stacking faults and turbostratic disorder, which occur frequently in the metastable structure because of the weak interactions between the lamellae.[12] When rapidly co-precipiated through direct ammonia addition, the product, **5**, does not show any notable long-range ordering by XRD (bottom pattern Figure 2). From this result, we conclude that the formation of the α-$Co(OH)_2$ structure is not favored relative to the direct precipitation of

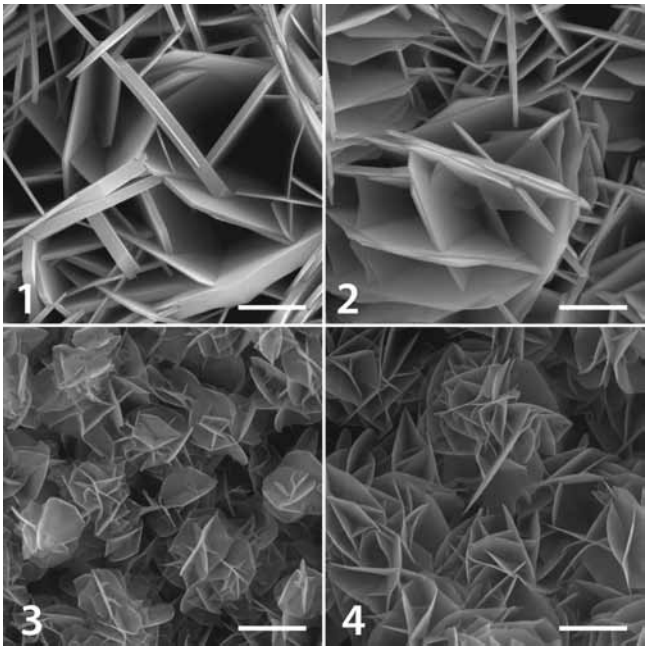

Figure 3. Scanning electron micrographs of compounds **1**−**4** illustrate changes of the average particle diameter and thickness, and the blunting of the platelet facets in progressively faster reactions from **1** to **4**. Scalebar 2 μm.

β-$Co(OH)_2$.[8,22] While the stoichiometry of these materials changes as a function of precursor hydrolysis and product formation rates, the average structure remains unchanged within the resolution of X-ray diffraction.

Electron microscopic examination of the hexagonal platelet morphology of compounds **1**−**4** shows characteristics consistent with those indicated by X-ray diffraction. Scanning electron microscopy (SEM) reveals that the slower reactions yield platelets (not to be confused with crystallites[10,23]) with sharper and thicker facets, indicative of improved long-range ordering (Figure 3). The upper left micrograph in Figure 3 shows that compound **1** is composed of platelets 5.0 ± 0.9 μm in diameter and 0.26 ± 0.13 μm in thickness. As the reaction rate increases (right and down in Figure 3), the platelets generally decrease in size: (**2**) 5.6 ± 0.8 μm diameter, 0.15 ± 0.08 μm thickness; (**3**) 2.3 ± 0.6 μm diameter, 0.033 ± 0.005 μm thickness; (**4**) 1.5 ± 0.2 μm diameter, 0.031 ± 0.005 μm thickness. Our observations from XRD and SEM are thus consistent with conventional wisdom that slower reactions extend long-range ordering,[24] but these analyses are insensitive to many crucial details about the local atomic structure of the materials.

Crystal structures of **1** and **4** were refined from powder diffraction profiles obtained with synchrotron radiation in transmission to eliminate artifacts from preferred orientations of the highly anisotropic powders. Both materials were refined to structures initialized with cobalt coordination site occupancies experimentally determined from this study (by EDS) and positions previously

(21) Stoch, J.; Capecki, A. *Surf. Interface Anal.* **1990**, *15*, 206–210.
(22) Gaunand, A.; Lim, W. L. *Powder Technol.* **2002**, *128*, 332–337.
(23) Schwenzer, B.; Pop, L. Z.; Neilson, J. R.; Sbardellati, T. B.; Morse, D. E. *Inorg. Chem.* **2009**, *48*, 1542–1550.
(24) Tiller,W. A. *The Science of Crystallization: Microscopic Interfacial Phenomena*; Cambridge University Press: New York, 1991.

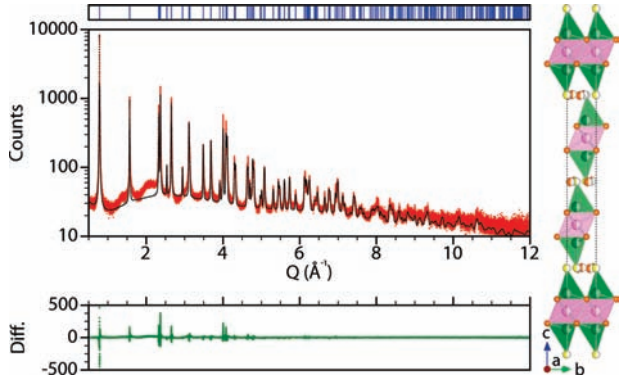

Figure 4. Synchrotron powder X-ray diffraction (APS, beamline 11-BM) of **1** (red dots) and calculated structure (black line) accompanied by the locations of major diffraction planes (blue hashes, top) and the difference profile (green line, bottom). A split atom model (right) of one unit cell of the calculated structure illustrates the $3R_1$ stacking polytype of the α-$Co(OH)_2$ with disordered occupancies of the cobalt, chlorine, and water atoms on average (pink: octahedral cobalt; green: tetrahedral cobalt; orange: oxygen; yellow: chlorine).

Table 2. Structure Parameters for Compound **1**, $Co_{1.2}(OH)_2(Cl)_{0.40}(H_2O)_{1.1}$, Obtained from High Resolution Powder X-ray Diffraction, Showing Fractional Coordinates (*x,y,z*), Occupancies (*g*), and Thermal Displacement Parameters (U_{11}) for a Rhombohedral Unit Cell, a = 3.138715(19), c = 24.05683(20), in the $R\bar{3}m$ (166) Space Group[a]

atom	site	*x*	*y*	*z*	*g*	U_{11}
Co^{oct}	3*a*	0	0	0	0.870(1)	0.00870(10)
Co^{tet}	6*a*	0	0	0.06938(9)	0.135(1)	0.01767(90)
OH	6*c*	1/3	−1/3	0.04655(5)	1	0.0215(4)
Cl	6*c*	0	0	0.16612(22)	0.135	0.0361(14)
H_2O	18*h*	0.1305(13)	−0.1305(13)	0.50199(129)	0.101(1)	0.0746(55)

[a] R_{wp} = 15:64%, R_p = 13:05%.

described[5] using the Rietveld method.[25] The refined structure of **1** (Figure 4, Table 2) has poor agreement with the analytically derived chemical formula (EDS, ICP), after refinement of the site occupancies (refined: $Co^{oct}_{0.87}Co^{tet}_{0.26}(OH)_2(Cl)_{0.26}(H_2O)_{0.6}$; analytical: $Co^{oct}_{0.80}Co^{tet}_{0.40}(OH)_2(Cl)_{0.40}(H_2O)1_{1.1}$. This highlights the insensitivity of X-ray diffraction to the precise coordination state of each cobalt atom and the disordered occupancy of each atomic position, as noted by the high thermal displacement parameters of the Co^{tet} and Cl sites in Table 2. The thermal displacement parameter for the water oxygen is also relatively high, as expected, since its position in the interlayer spacing is variable in the lattice. It also is important to point out that no reflections appear from long-range ordering of the tetrahedral sites in the lattice, as observed in the zinc analogue, $Zn_5(OH)_8(Cl)_2(H_2O)$.[6] Therefore, our choice of a smaller unit cell with split site occupancies for the tetrahedral and octahedral cobalt positions is better suited for these compounds to accommodate the positional and occupational disorder of cobalt sites. Overall, there is great agreement with the previously reported structure for the chloride containing α-$Co(OH)_2$;[5] however, these results illustrate the insensitivity of the average structure to the precise occupancy of each site, despite the high apparent crystallinity and high quality of the data.

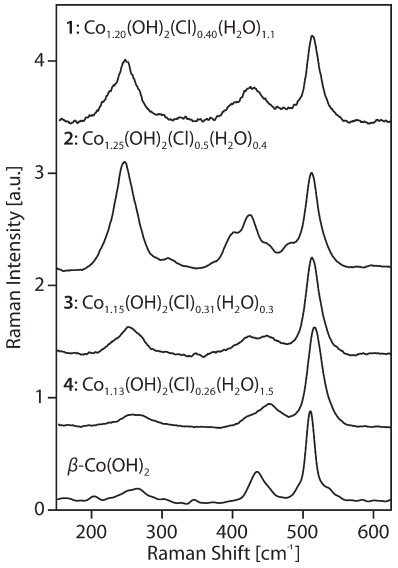

Figure 5. Raman spectra of compounds **1**−**4** and β-$Co(OH)_2$ illustrating additional vibrational modes scaling with chloride content, attributed to 4-coordinated cobalt sites of C_{3v} symmetry.

When analyzing the synchrotron X-ray diffraction pattern from compound **4** (Supporting Information, Figure S3), it is difficult to accurately represent the asymmetric peak broadening typically seen in lamellar materials as a result of the large concentration of stacking faults and turbostratic disorder.[2,12] As such, quantitative refinement of the occupancies and thermal parameters is unreliable for **4** (Supporting Information, Figure S3). However, these data indicate the average structure is highly related to compound **1**, as no reflections are absent or extra. These results also provide evidence of structural homogeneity without impurity phases such as the β-$Co(OH)_2$.

Intralayer Structure. Traditional powder X-ray diffraction cannot be used to accurately determine the occupancy or intermediate range ordering of the tetrahedral sites in the layered lattice (Figure 2). This is hindered by the long-range disorder in the lattice introduced by stacking defects, the insensitivity to low-mass elements surrounding the metal sites, and positional disorder in the lattice. Short-range structural characterization methods are needed to probe the intralayer structure. We therefore used vibrational spectroscopy to identify the local structure of the cobalt−oxygen cages.

Raman active vibrations in the range of 150−625 cm^{-1} identify the local symmetries of metal−oxygen complexes within the lattice.[26] Using β-$Co(OH)_2$ to aid in peak assignment, as it has only 6-coordinated cobalt atoms in the lattice (D_{3d} symmetry), four Raman modes are observed (Figure 5), with two modes at 250 and 427 cm^{-1}, attributed to $E_g(T)$ and $A_{1g}(T)$ vibrations, and two modes centered at 510 and 522 cm^{-1}, from $A_{2u}(T)$ and $E_g(R)$ vibrations.[27] A qualitative comparison between β-$Co(OH)_2$ and compounds **1**−**4** confirms that faster reactions yield materials more closely related to the all-octahedral-containing β-$Co(OH)_2$. As more 4-coordinated cobalt

(25) Rietveld, H. M. *J. Appl. Crystallogr.* **1969**, *2*, 65–71.

(26) *Solid state chemistry: Techniques*; Cheetham, A. K., Day, P., Eds.; Oxford University Press: New York, 1987.

(27) Shieh, S.; Duffy, T. *Phys. Rev. B* **2002**, *66*, 134301.

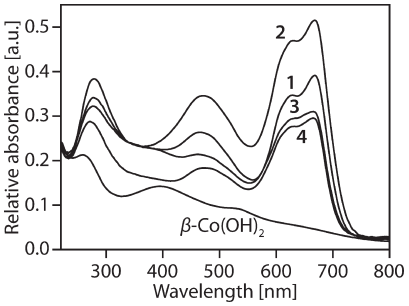

Figure 6. UV−visible diffuse reflectance spectra of compounds **1**−**4** and β-$Co(OH)_2$ illustrating an increase in the tetrahedral cobalt absorbance at 640 nm as a function of chloride content.

sites are populated in the slower reactions, additional modes appear, likely from the addition of a C_{3v} symmetry with two Raman modes, E and A_1. No specific assignments are made to these peaks, as no well-characterized cobalt hydroxide compounds containing solely tetrahedral coordination exist for comparison. However, we observe a pronounced, systematic incease in deviation from the spectrum of β-$Co(OH)_2$ with additional chloride content. Therefore, vibrational spectroscopy also indicates modulation of the population of C_{3v} species, inversely proportional to the occupancy of D_{3d} sites, as controlled by the reaction kinetics.

Diffuse reflectance spectroscopy provides complementary evidence for a characteristic electronic structure in support of this conclusion. Tetrahedrally coordinated Co^{2+} (d^7) lacks a center of symmetry and d-d transitions are permitted. This is in contrast to octahedral Co^{2+}, in which d-d transition are Laporté forbidden, providing a sensitive optical probe of tetrahedral cobalt ions.[7] The measured absorbance spectra of compounds **1**−**4** in Figure 6 show strong bands at 625 and 665 nm, characteristic of $[Co(OH)_3Cl]^{2-}$ complexes in the lattice, giving the material its distinctive green color.[5,7] This absorbance band is absent in the β-$Co(OH)_2$ compound, which is characteristically pink in color. Additionally, there are no strong and broad absorption bands indicating the presence of the highly absorbing low-spin Co^{3+}-(d^6). The 625 and 665 nm absorption bands increase in intensity from compound **4** to **3** to **2**, with a decrease to **1**, reflecting the same trend of tetrahedrally coordinated cobalt ion concentration previously observed in both the chloride content and the Raman spectroscopy.

Proposed Mechanism. Examination of the partial charges and stability of the aqueous precursor complexes explains the direct kinetic control of the atomic structure of the final product by the hydrolysis rate. The partial charge model, described by Livage et al.,[28] assumes that the structures of stable aqueous complexes of the metal salts are determined by the pH-dependent mean electronegativity of the bulk solvent. The number of bound hydroxyl ligands, h, of a cobalt hexaquo complex, $[Co(H_2O)_6]^{2+}$, follows an increasing function of pH,

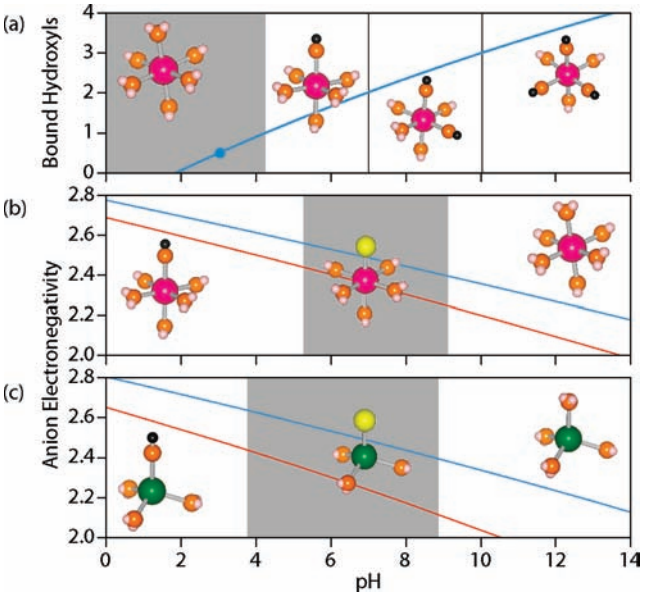

Figure 7. Partial charge calculations and schematic representations of predicted pH dependent aqueous cobalt complexes (pink: octahedral cobalt, green: tetrahedral cobalt, orange: oxygen, yellow: chlorine, white: water hydrogen, black: hydroxyl hydrogen). Gray boxes indicate predicted soluble complexes. (a) Bound hydroxyls (h) of a cobalt hexaquo complex as a function of solution pH. Blue circle denotes pH of precursor solution. (b-c) Anion electronegativity−pH relationships of (b) octahedral $[Co(H_2O)_5Cl]^+$ and (c) tetrahedral $[Co(H_2O)_3Cl]^+$ complexes. Hydrolytic dissociation occurs at lower pH values (red lines, $q = 1$) when the partial charge of the anionic ligand matches that of the protonated ligand HCl (electronegativity of 2.44); Anionic dissocation prevails at higher pH values (blue lines, $q = 0$) when the anionic partial charge reaches that of the deprotonated ligand, $Cl^-_{(aq)}$ (electronegativity of 2.39). (See details in the Supporting Information.).

shown graphically in Figure 7a, and described analytically in the Supporting Information.[29] The initial pH of the pink 0.1 M $CoCl_{2(aq)}$ solution is 3.0. The characteristic pink color is indicative of an octahedral cobalt(II) hexaquo complex,[7] and the decreased pH results from spontaneous partial hydrolysis of a non-stoichiometric amount of bound water, in agreement with this predictive model and prior work.[30] However, these complexes remain soluble only at low pH, as indicated in gray in Figure 7a, as the partial charge model predicts that spontaneous olation only occurs with an average hydrolysis ratio of one for divalent cobalt.

As the pH slowly increases in response to the slow diffusion of the ammonia vapor, the number of hydroxyl ligands, h, is predicted to increase according to the calculated curve until $h = 1$, permitting spontaneous olation above pH 4.3, to yield $[Co(OH)(H_2O)]^+$. At this point, it is important to consider the role of the chloride counteranion. According to the partial charge model, $[Co(H_2O)_5Cl]^+$ complexes are stable only in the pH range between 5.3 and 9.1 (Figure 7b and Supporting Information). At lower pH, the increased anion electronegativity favors hydrolytic dissociation of the chloride complex, to form $[Co(OH)(H_2O)_5]^+$ when the partial charge of the chloride ligand matches the mean electronegativity of HCl. Anionic dissociation, which yields $[Co(H_2O)_6]^{2+}$, occurs at higher pH because the partial

(28) Livage, J.; Henry, M.; Sanchez, C. *Prog. Solid State Chem.* **1988**, *18*, 259–341.

(29) Henry, M.; Jolivet, J.-P.; Livage, J. Aqueous chemistry of metal cations: Hydrolysis, condensation and complexation. In *Chemistry, Spectroscopy and Applications of Sol-Gel Glasses*; Springer: Berlin, 1992; Vol. *77*, pp 153−206.

(30) Baes, C. F.; Mesmer, R. E. *The Hydrolysis of Cations*; Wiley: New York, 1976.

charge of a complexing chloride equals the mean electronegativity of $Cl^-_{(aq)}$ (Figure 7b).[29] At pH 4.3, the equilibrium of $[Co(H_2O)_5Cl]^+$ formation is shifted toward hydrolytic dissociation, preventing association of the chloride ligand. However, tetrahedral $[Co(H_2O)_3Cl]^+$ complexes are predicted to be stable from $3.8 < pH < 8.9$, without hydrolytic or anionic dissociation (Gray box, Figure 7c). At a pH below 3.8, no cobalt chloride complexes are stable, according to this model.

As described above, the stability range of the tetrahedral complex, $[Co(H_2O)_3Cl]^+$, extends to lower pH than the onset of hydrolysis, which yields $[Co(OH)(H_2O)_6]^+$. This predicts that the probability of forming metal chloride complexes is more likely when the pH is slowly elevated, as the equilibrium constant for complex formation in a dilute solution is low ($K_f = 4.9$).[31] During olation, the nucleophilic attack of the hydroxyl ligand from a $[Co(OH)(H_2O)_6]^+$ complex on a transiently formed cobalt trisaquo chloride species can trap the tetrahedral structure into an oligomeric cluster, which continues to form the insoluble lattice with mixed metal coordination sites. This situation is predicted to occur during intermediate hydrolysis conditions (forming compounds **4**, **3**, then **2**), when the predicted soluble metal complexes are either $[Co(OH)(H_2O)_5]^+$ species or $[Co(H_2O)_3Cl]^+$. In aqueous solution, Co^{2+} has a solvent exchange rate of $\sim 2 \times 10^6\ s^{-1}$.[32] The rate of Brownian motion is approximated to a time scale of $\sim 1 \times 10^9\ s^{-1}$, by considering a cross-section of solution corresponding to the area of a soluble oligomer ($< 1\ nm^2$).[33] Since molecular diffusion on this length scale is faster than the rate of solvent exchange, there is an increased probability that these two complexes will collide and condense via olation to form an oligomeric cluster containing both metal coordination environments. However, under slow hydrolysis conditions leading to the formation of compound **1**, there is sufficient time for solvent exchange and complex rearrangement before olation, permitting a closer approach to equilibrium, and stabilization of the octahedral complexes. Therefore, the number of tetrahedral sites decreases, as seen in **1**, with a structure closer to β-$Co(OH)_2$, as produced under near equilibrium conditions without kinetic control.[8,22] This rationale involving the role of the counteranion and the competing kinetic processes provides a simple and generic explanation for the observed systematic dependence on hydrolysis rate of the final chloride incorporation in the lattice, and the population of tetrahedrally coordinated cobalt. The use of simple reagents bearing the active anionic solute in conjunction with control of the rate at which the hydrolytic catalyst is introduced provides a powerful method for synthesizing a wide array of different metastable structures, with well-defined short and long-range ordering.

Conclusions

The first conclusion of this study shows that the α-$Co(OH)_2$ structure for cobalt hydroxide chloride is flexible; the occupancy of the tetrahedrally coordinated cobalt is a variable. Second, the ratio of octahedrally coordinated to tetrahedrally coordinated cobalt is controlled by the hydrolysis and condensation kinetics. The cobalt−oxygen coordinations and overall compositions are independently investigated to observe systematic changes that do not significantly alter the average structure of the material. This yields the conclusion that faster reactions introduce fewer tetrahedral sites into the lattice when synthesis occurs in the kinetically controlled regime. However, very slow reactions approach equilibrium conditions departing from kinetic control, also depopulating tetrahedrally coordinated cobalt sites. A simple model of the soluble precursor complexes involving an active role of the solute counteranions supports our experimental observations of a direct influence of the reaction rate on the ratio of tetrahedrally to octahedrally coordinated metal sites in the layered hydroxide salt. This result emphasizes the need for rigorous structural characterization to understand the role of short and intermediate range order of layered compounds produced by cooperative and competing processes.

Acknowledgment. The authors thank B. Melot, J. Kurzman, R. Feller, T. Mates, Y. Li, and M. Divinigracia for helpful discussions regarding experimental methods and the expert beamline staff of 11-BM at APS for their expedient service. Use of the Advanced Photon Source was supported by the U.S. Department of Energy, Office of Science, Office of Basic Energy Sciences, under Contract No. DE-AC02-06CH11357. This work was supported in part by grants from the U.S. Department of Energy (Grant DE-FG02-02ER46006), the U.S. Army Research Office (through Contract No. W911NF-09-D-0001 to the Institute for Collaborative Biotechnologies), the National Science Foundation (through a Graduate Research Fellowship to J.R.N.), and the facilities of UCSB's Materials Research Laboratory (through the NSF's MRSEC Program Grant DMR05-20414).

Supporting Information Available: Additional characterization and explanation of the partial charge model.[29] This material is available free of charge via the Internet at http://pubs.acs.org.

(31) Atkins, P.; Overton, T.; Rourke, J.; Weller, M.; Armstrong, F. *Inorganic Chemistry: Shriver & Atkins*, 4th ed.; Oxford University Press: New York, 2006.
(32) Burgess, J. *Metal Ions in Solution*; Ellis Horwood: New York, 1978.
(33) Geankoplis, C. J. *Transport processes and Separation Process Principles* (*Includes Unit Operations*); Prentice Hall: New York, 2003.